Science
AAAS

Supplementary Materials for

Prenatal activity from thalamic neurons governs the emergence of functional cortical maps in mice

Noelia Antón-Bolaños[†], Alejandro Sempere-Ferràndez [†], Teresa Guillamón-Vivancos, Francisco J. Martini, Leticia Pérez-Saiz, Henrik Gezelius, Anton Filipchuk, Miguel Valdeolmillos, Guillermina López-Bendito[*]

[*]Corresponding author. E-mail: g.lbendito@umh.es

This PDF file includes:

Other Supplementary Materials for this manuscript include the following:

Materials and Methods

Mouse strains

All transgenic animals used in this study were maintained on an ICR/CD-1 genetic background and genotyped by PCR. The day of the vaginal plug was stipulated as E0.5. The *R26*^{tdTomato} Cre-dependent mouse line was obtained from Jackson Laboratories (Stock number 007908). The *TCA-GFP Tg*, in which the TCAs are labeled with GFP (*19*), and the *R26*$^{Kir2.1\text{-}mCherry}$ (*10*) mouse lines were previously described. The *R26*^{GCaMP6f}, a Cre-dependent mouse line, was obtained from Jackson Laboratories (Stock number 024105) and crossed with an *Emx1*$^{Cre/+}$ transgenic mouse (*27*) to conditionally express the fast calcium indicator GCaMP6f in glutamatergic cortical neurons. The *Thy1-GCaMP6f* mouse line (Jackson Laboratories, 025393) expresses GCaMP6f in excitatory neurons of the brain. In this mouse line, the expression of GCaMP6f in the cortex switches on at perinatal stages, and increases its expression to cover the entire primary somatosensory cortex (S1) postnatally. The *R26*$^{Kir2.1\text{-}mCherry}$, *R26*^{tdTomato} and *R26*^{GCaMP6f} floxed mice were crossed with an inducible *Cre*^{ERT2} mouse line driven by *Gbx2,* an early specific thalamic promoter (*Gbx2*$^{CreERT2/+}$) (*28*). Double mutants are referred as *Th*^{Kir}, *Th*^{tdTomato} and *Th*^{GCaMP6f}, respectively. We also generated the following triple mutants: *TCA-GFP-Th*^{Kir} and a *Thy1-GCaMP6f-Th*^{Kir}. Tamoxifen induction of Cre recombinase in the double/triple mutant embryos was performed by gavage administration of tamoxifen (5 mg dissolved in corn oil, Sigma) at E10.5 to specifically target all primary sensory thalamic nuclei. Tamoxifen administration in pregnant mice produces non-desirable side effects such as delivery problems and decrease survival of newborn pups (*29*). In order to increase the survival rate of young pups, we administered 125 mg/Kg of progesterone (DEPO-PROGEVERA®) intraperitoneally at E14.5 and implemented C-

section procedure at E19.5. Pups were then placed with a foster mother. In all cases, the Cre^{ERT2}-negative littermates were used as controls of the experimental condition.

The Committee on Animal Research at the University Miguel Hernández approved all the animal procedures, which were carried out in compliance with Spanish and European Union regulations.

Immunohistochemistry and cytochrome oxidase staining

For immunohistochemistry at postnatal stages, mice were perfused with 4% paraformaldehyde (PFA) in PBS (0.01 M), and the brains were dissected and post-fixed overnight. Embryonic brains were directly dissected and fixed in 4% PFA overnight. For cytochrome Oxidase (CytOx) staining, coronal sections were incubated overnight at 37 ºC in a CytOx solution: 0.03% cytochrome c (Sigma), 0.05% 3-3′ diaminobenzidine tetrahydrochloride hydrate (DAB, Sigma #D5637) and 4% sucrose in PBS. For tangential sections, cortical hemispheres were flattened and cryoprotected through steps of 10%, 20% and 30% of sucrose in PBS. Then, a cryotome (MICRON) was used to cut at 80-100 µm tangential sections. Immunohistochemistry was implemented on 60-100 µm vibratome or cryotome brain sections (coronal and tangential) that were first incubated for 1h at room temperature in a blocking solution containing 1% BSA (Sigma) and 0.3% Triton X-100 (Sigma) in PBS. Afterwards, the slices were incubated overnight at 4 °C with the following primary antibodies: guinea pig anti-vGlut2 (1:5000, Synaptic Systems, #135404), chicken anti-GFP (1:3000; Aves Labs, #GFP-1020)**,** rat anti-RFP (1:1000 Chromotek, #5F8), mouse anti-NeuN (1:1000 Merk-Millipore, #MAB377), rabbit anti-Cux1 (1:500, Santa Cruz #13024), rabbit anti-cFos (Synaptic Systems, #226003) and guinea pig anti-cFos (Synaptic Systems, #226004). Sections were then rinsed in PBS and incubated for 2h at room temperature with secondary antibodies: Alexa488 donkey anti-guinea pig (1:500, ThermoFisher, #A11073), Alexa546 donkey anti-guinea pig (1:500, ThermoFisher, #A11040), Alexa488 goat anti-chicken (1:500,

ThermoFisher, #A11039), Alexa594 donkey anti-rat (1:500, ThermoFisher, #A21209) and the biotinylated secondary antibody anti-rabbit (1:500, Vector labs #BA-1000). Sections were counterstained with the fluorescent nuclear dye DAPI (Sigma-Aldrich). When signal amplification was required**,** sections with biotinylated secondary antibodies were incubated with Avidin–Biotin Complex (ABC 1:500, Vectastain #PK-6100) for 1 h 30 min, washed in PBS-T and Tris-HCl 0.05 M pH 7 and revealed in Tris-HCl 0.05 M with 0.05% DAB and 0.18% H_2O_2.

Slice preparation for calcium measurements

The brains of embryonic or postnatal mice (E16.5-P8) were dissected out rapidly and immersed in an ice-cold slicing solution containing (in mM): 2.5 KCl, 7 $MgSO_4$, 0.5 $CaCl_2$, 1 NaH_2PO_4, 26 Na_2HCO_3, 11 Glucose and 228 Sucrose. Brain hemispheres were separated through the midline, and 350-450 µm thick slices were obtained from each half in a vibratome (VT1200 Leica Microsystems Germany). To preserve thalamocortical connectivity from the ventral postero-medial nucleus (VPM) to S1, a cutting angle of 45º was employed. Slices recovered during 30 min at room temperature in standard ACSF containing (in mM): 119 NaCl, 5 KCl, 1.3 $MgSO_4$, 2.4 $CaCl_2$, 1 NaH_2PO_4, 26 Na_2HCO_3 and 11 glucose. All extracellular solutions were continuously bubbled with a gas mixture of 95% O_2 + 5% CO_2.

Ex vivo calcium imaging

Slices were loaded with the calcium indicator Cal520^{TM} (AAT Bioquest) as previously described (*10*), transferred to a submersion-type recording chamber and perfused with warmed (32-34 ºC) ACSF at a rate of 2.7-3.5 ml min^{-1}. Images were acquired with a digital CCD camera (Hamamatsu ORCA-R2 C10600-10B) coupled to a Leica DM-LFSA microscope using 5x or 20x water immersion objectives. For recordings of spontaneous calcium activity, frames were acquired with

an exposure time of 150 ms, an interframe interval of 300 ms, a frame size of 672x512 pixel and a spatial resolution of 2.5μm/pixel. With each slice, 1 to 5 epochs of 15 mins (3000 frames) were recorded. For evoked responses, images were acquired with an interframe interval of 100-250 ms and an exposure time of 50-150 ms. For selective blockage of mGlu5 receptors, 2-Methyl-6-(phenylethynyl)pyridine (MPEP, Tocris #1212) was used.

In vivo calcium imaging

At E18.5, embryos were retrieved from the dam's uterus through C-section, kept at 37 ºC and immobilized with soft clay. At P3-P4, mice were anesthetized in ice and their scalp removed. A 3D-printed plastic holder was glued to the skull with cyanoacrylate adhesive and dental cement and attached to a ball-joint holder to immobilize the head. At P3-P4, pups body temperature was kept at around 25 ºC to provide weak anesthesia. Whisker pad stimulation was performed using a 0.16 g von Frey filament (Touch Test®, BIOSEB). To record the calcium responses, we used a 16-bit CMOS camera (Hamamatsu ORCA-Flash 4.0) coupled to a fluorescence stereo microscope (M165FC, Leica). To visualize the whole head, images were acquired at 2.5x zoom and 3.33Hz frequency of acquisition. The frame size was 2048x2048 pixel (6.67x6.67 μm/pixel) for the E18.5 mice and 1024x1024 pixel (12.82x12.82 μm/pixel) for the P3-P4 mice.

Electrical stimulation

Slices were stimulated with a low resistance glass pipette filled with ACSF (0.6-0.8 kΩ). Single, monopolar current pulses (intensity 25-500 μA, duration 0.2 ms) were delivered by a stimulus isolator (Iso-Flex, AMPI) coupled to a computer trough an A/D converter (Digidata 1550-B, Molecular Devices) and controlled by the pulse-generator tool of pClamp 10.6 software (Molecular Devices). The return was trough a low impedance electrode in the bath.

Whole-cell recordings *ex vivo*

Somatic whole-cell recordings from VPM/subplate/cortical neurons were made under visual control using an upright microscope (Leica DM-LFSA) and a water immersion objective (40x). The intracellular solution contained (in mM): 130 K-gluconate, 5 KCl, 5 NaCl, 0.2 EGTA, 10 HEPES, 4 MgATP and 0.4 NaGTP; pH 7.2 adjusted with KOH; 285-295 mOsm. To mimic the expected higher concentration of intracellular Cl^- in early stages of development (*30*), a high-Cl intracellular solution was employed for thalamic embryonic slices (in mM): 90 K-gluconate, 44 KCl, 1 $CaCl_2$, 2 $NaCl_2$, 11 EGTA, 10 HEPES, 2 MgATP and 0.5 NaGTP. Recordings were obtained in current-clamp and/or voltage-clamp mode with a patch-clamp amplifier (Multiclamp 700A, Molecular Devices). No correction was made for the pipette junction potential, which was estimated at -10 mV using the junction potential calculator from pClamp. Voltage and current signals were filtered at 2-4 kHz and digitized at 20 kHz with a 16-bit resolution A/D converter (Digidata 1550-B, Molecular Devices). The generation and acquisition of pulses were controlled by pClamp. Patch pipettes were made from borosilicate glass (1.5 mm o.d., 0.86 mm i.d., with inner filament) and had a resistance of 4-7 MΩ when filled. In current-clamp experiments, series resistance (R_s) was measured and balanced on-line under visual inspection assisted by the Bridge Balance tool of pClamp software. R_s was monitored at the beginning and at the end of each protocol, and re-balanced if needed. In voltage-clamp experiments, the error in the measured membrane potential (V_e) was computed as $V_e = I_{hold} \times R_s$ and subtracted off-line from the holding potential (V_{hold}); I_{hold} stands for the holding current needed to set V_{hold}. Recordings with R_s >30 MΩ were discarded. Quantification of intrinsic membrane properties and spontaneous neuronal activity was performed on Clampfit 10.7 (Molecular Devices).

In vivo extracellular recordings

P2-P3 mice were anesthetized on ice, then the scalp was removed and the skull cleaned. A 3D-printed holder was glued to the skull by cyanoacrylate adhesive and dental cement, and attached to a stereotaxic apparatus. A 2x2 mm craniotomy was made over the left hemisphere, leaving the dura mater intact. The craniotomy revealed a window above the barrel field in S1 (0-0.5 mm posterior to bregma and 1.5-2.0 mm from the midline) or in the area of the VPM (1.8 mm anterior to lambda and 2.0 mm from the midline), allowing the perpendicular insertion of the multi-channel electrodes. During recordings, mice were kept warm (36-37 °C) by using a heating blanket and lightly anesthetized with isoflurane (0.5%). Local field potential (LFP, 1-100Hz) was recorded using 4-shank/16-channel silicon probes, with an inter-electrode distance of 50 μm and an inter-shank distance of 200 μm (E16+R-50-S4-L6-200NT, ATLAS). Multi-unit activity (MUA, >300Hz) was recorded with a linear electrode of 16 channels separated by 50 μm (E16+R-50-S1-L6NT, ATLAS). Shank trajectories were stained with DiI (1,1′-dioctadecyl 3,3,3′,3′-tetramethylindocarbocyanine perchlorate; Invitrogen) diluted in 70% alcohol. Probes were inserted perpendicular into S1, 300-400 μm deep across the cortical layers for S1 and 2800-3000 μm deep for VPM recordings. The electrical signal activity was sampled at 20 kHz by a filter amplifier and visualized using MC_RACK software (Multi Channel Systems). Whisker stimulation was performed by applying a brief (30 ms) air puff (20 repetitions every 4 seconds). After the recording sessions, brains were dissected out and fixed with 4% PFA overnight. In order to determine the position of every channel, 100 μm-thick coronal sections were cut and counterstained with the fluorescent nuclear dye DAPI.

Data analysis was made using Matlab^{TM} routines. The LFP was calculated for each channel and 4 sec epochs of activity were extracted using a threshold-based detection (threshold: 3 times

baseline standard deviation). For each epoch detected, the electrode with maximum amplitude in each shank was selected and, among them, the electrode of the shank with the strongest signal was picked to calculate cross-correlations against it. Cross-correlations analysis was performed using a temporal window of +/- 2 seconds and then correlation coefficients were averaged in 250 ms bins. In this way, four values were obtained per mouse, one for the auto-correlation (set as distance = 0 μm) and three for correlations with other shanks (up to 600 μm if the strongest response was in a lateral most shank, number 1 or 4). Population averages were calculated from mice averages.

Analysis of fluorescence spontaneous activity

Analysis of spontaneous thalamic calcium activity was performed using custom software written in Matlab™ adapted from the CalciumDX toolbox (available at https://github.com/ackman678/CalciumDX). For each movie, VPM was delineated and the area divided into a grid of 6x6 pixels where each small square is a region of interest (ROI). Events of calcium activity were detected from the average calcium signal of each ROI as a function of time using threshold-based algorithms modified from CalciumDX. To identify significant synchronous activity and discard ROI co-activation that emanates from random temporal coincidence of calcium events, we created surrogated calcium events sequences in Matlab™ for each experiment. The alternative dataset was built by shuffling randomly the original temporal intervals between calcium transients in every ROI. In this way, the spiking frequency and temporal structure of the calcium activity was preserved. Next, the maximum value of co-activation from shuffled data was calculated. After 1000 iterations, we were able to define a synchronicity threshold as the 95th percentile of the maximum values of co-activation obtained from the shuffled dataset. In each experiment, only activity above the synchronicity threshold was used for calculations and plotting. The beginning of a synchronic event is defined as the frame in which co-activation overpass the

threshold and the end is defined as the frame in which co-activation reached 25% of peak synchronicity.

Analysis of fluorescence evoked activity in slices

Data analysis was performed in ImageJ (NIH). Stimulus-locked temporal stacks of $\Delta F/F_0$ were computed using a 1.5 s time window prior to stimulus application (F_0). In each slice, 5-8 stimulus intensities were tested (2 pulses with inter-stimulus interval of 30 s for each intensity; 5 min inter-stimulus interval within intensities) and an input/output (I/O) curve was generated. The total area activated was quantified for each stimulus intensity. Threshold intensity was defined for each slice as the minimum stimulation current that elicited a measurable calcium response ≥ 0.01 $\Delta F/F_0$ at the response origin site (either the subplate or layer 4, depending on the age). The average threshold intensity across ages and genotypes was 127 ± 8 μA. Slices were discarded if threshold intensity ≥ 300 μA. Peri-threshold stimulation intensity was ≤ 50 μA above threshold. The average peri-threshold intensity was 159 ± 9 μA, 32 ± 4 μA above threshold. In Figure 3C and Figure S6D, two stimulus intensities (within the rising phase of the I/O curve and in the plateau of the I/O curve) were sampled for each slice. Response origin was measured as the $\Delta F/F_0$ of a 50 μm width column occupying the entire cortical depth and centred in the cortical response initiation site ($\Delta F/F_{0,origin}$). Horizontal spreading of the response within the cortex was determined by computing the distance from response origin at which $\Delta F/F_0$ in the column dropped to 50% [distance ($0.5*\Delta F/F_{0,origin}$)]. This was quantified for both sides from the response initiation, referred as + and – sides. In some experiments, and due to the thickness of the slice, a calcium signal appears beyond the pial surface.

Analysis of fluorescence signals from *in vivo* experiments

Image analysis was performed on ImageJ (NIH). An average of 3-4 images just prior to the stimulation was used as F_0. $\Delta F/F_0$. Time-series were transformed into 8-bit images and processed with a 2-pixel diameter Gaussian filter. The maximum intensity projection of all frames with activated cortical areas was obtained. The wand tool was used to delineate the ROI with a perimeter of pixels of the same intensity level. In Figure 4D the white lines delimiting ROI # 3 (pink) represent the maximum extension of the activity, covering 6 frames in the control and 8 frames in the Th^{Kir}.

Dye-tracing studies

For axonal tracing, animals were perfused with 4% PFA in PBS, and their brains dissected out and post-fixed overnight. In order to trace VPM thalamocortical axons, a DiD crystal (1,1'-dioctadecyl-3,3,3',3'-tetramethylindodicarbocyanine, 4-chlorobenzenesulfonate salt, Invitrogen) was inserted into the VPM at E17.5. In order to trace the corticothalamic pathway small DiI and DiA (4-[4-(dihexadecylamino) styryl]-N-methylpyridinium iodide, Invitrogen) crystals were inserted under a stereo fluorescence microscope (Leica MZ10 F) into distinct barrels: C1 and C4. To reveal the PBMSF, a TCA-GFP transgenic specific animal line was used. To back-label the thalamocortical pathway, fixed brains were embedded in 3% low melting agarose and cut coronally from caudal to rostral until the VPM was exposed. Dye crystals were then placed in the VPM and allowed to diffuse at 37 °C in PFA solution for 1-4 weeks. Vibratome sections (60-100 μm) were obtained and counterstained with the fluorescent nuclear dye DAPI. Image analysis was performed on ImageJ (NIH). A ROI of 250 μm long x 50 μm width was located in the centre of every barrel analysed in control animals. For Th^{Kir} mice the ROI was located in centre of layer 4. In order to quantify the difference in the fluorescence intensity, the 250 μm analysed were divided in 10 bins

of 25 μm each. Fluorescence signal was normalized in every individual by its maximum. The graph in Figure S14 represents the average fluorescence intensity per bin.

Novelty Exposure experiments

Novelty exposure experiments were done in adult mice (~P60). The day before the experiment, mice were initially habituated to the room (light conditions, space and odorants), to the researcher and for 30 min to the open field empty box. Afterwards, the whiskers of the snout were either completely trimmed or the C2 whisker spared. Next day, the mouse was deposited in the open field box with objects. Mice were free to investigate novel objects for 1 hour while their track was recorded. Immediately after, intracardiac perfusion was carried out and brain dissected and post-fixed overnight. For cFos immunostaining, coronal sections of 50-70 μm were cut in a vibratome or tangential flattened sections obtained by a cryotome.

Statistics

Statistical analysis was carried out using GraphPad Prism6^{TM}, Matlab^{TM} and OriginPro 2018^{TM}. Statistical comparison between two populations was performed using unpaired two-tailed Student's *t*-test with Welch correction (equal variance not assumed) or Mann-Whitney *U*-Test non-parametric two-tailed test when data failed Kolmogorov-Smirnov normality test. For more than two populations and one factor, one-way ANOVA was used combined with Tukey post hoc analysis. In these analyses, P values < 0.05 were considered statistically significant and set as follows $*P < 0.05$; $**P < 0.01$ and $***P < 0.001$. Dependent variables sampled at different age groups and genotypes were independently compared at each age across genotype with a Student's *t*-test or the Mann-Whitney *U*-test followed by the false discovery rate (FDR) procedure (*31*). In this case, thresholds for significance were computed according to the FDR method and are referred in the "Quantifications" section below. For analysis of the horizontal extension of cortical

responses after thalamic or intracortical stimulation, both flanks splitting away from the response initiation site where considered as independent variables. However, when the total extension was used as a single variable (including both sides), the statistical result was not affected. No statistical methods were used to predetermine the sample size, but the number of samples are considered adequate for our experimental designs and consistent with the literature. The mice were not randomized. The investigators were blinded to sample identity except in calcium activity experiments.

Microdissection, purification of total RNA and quantitative real-time PCR

Tissue microdissection, RNA extraction and qPCR protocols were previously described (*10*). *mGlu5* (Gene ID: 2915) gene expression was determined by the primers 5'-GCACGTAGGCAAGTCATC-3' and 5'-GGGTTCTCCTTCTTGTTGATATGG-3'. The housekeeping gene Gapdh was used as a control, (Gene ID: 14433) and determined by the primers 5' CGGTGCTGAGTATGTCGTGGAGT-3' and 5'- CGTGGTTCACACCCATCACAAA-3'.

Quantifications

Main Figures

In Fig. **1A**, stimulus intensity 125 μA, stimulus duration 0.2 ms.

In Fig. **2B**, mean event amplitude ($\Delta F/F_0$): one-way ANOVA test F = 14.48, ***P <0.001; Tukey's multiple comparison test post-hoc analysis **P < 0.01, ***P < 0.001, ns-not significant, P = 0.785). Mean event frequency: one-way ANOVA test: F = 8.606, **P <0.01; Tukey's multiple comparison test post-hoc analysis *P < 0.05, **P < 0.01; ns. P = 0.608). Event duration: one-way ANOVA test: F = 3.44, P = 0.053. Tukey's multiple comparison post-hoc analysis: control vs Th^{Kir} *P < 0.05, control vs $control_{low\text{-}synch.}$ P = 0.463 and $control_{low\text{-}synch.}$ vs Th^{Kir} P = 0.437. In Fig. **2D,** one-way ANOVA F = 132.0, *** P < 0.001: Tukey's multiple comparison test: control

vs Th^{Kir} state1 ns. $P = 0.277$; control vs Th^{Kir} state2 ***$P < 0.001$; Th^{Kir} state1 vs Th^{Kir} state2 ***$P < 0.001$.

In Fig. **3A**, Student's *t*-test. ns. $P = 0.16$. In Fig. **3C**, left panel, quantification of the horizontal spreading. Bars represent the extent of activation from the start of the field of increased calcium to the lateral edges, measured as the point where fluorescence is 50% with respect to the initiation site. Red points lying beyond the vertical dashed lines correspond to Th^{Kir} calcium waves that spread out of the imaged field (± 750 μm from the origin). Student's *t*-test or Mann-Whitney test p-value for + side spreading: E17-18 <0.001, P0-1 0.006, P2-3 0.007, P4-7 0.052, and for – side spreading: E17-18 0.005, P0-1 0.005, P2-3 <0.001, P4-7 0.034; all these comparisons are significant after FDR correction for multiple comparisons with the exception of + side P4-7. Right panel: Two-way ANOVA test: $F_{genotype} = 60.85$, ***P <0.001. In Fig. **3F**, Two-way ANOVA test: $F_{genotype} = 8.91$, **P <0.01.

In Fig. **4A**, control and Th^{Kir}, $n = 6$. In Fig. **4D**, area normalized to controls. Mann-Whitney *U*-test. In Fig. **4E**, control and Th^{Kir}, $n = 5$. In Fig. **4F**, control and Th^{Kir}, $n = 3$.

Supplementary Figures

In Fig. **S1C**, one-way ANOVA test: F = 5.808, ***P <0.001. Tukey's multiple comparison test (post-hoc analysis).

In Fig. **S2B**, $n = 6$. In Fig. **S2C**, left: $n = 10$, right: $n = 3$. In Fig. **S2D**, $n = 4$.

In Fig. **S3B**, Student's *t*-test.

In Fig. **S4B**, Student's *t*-test corrected with the FDR procedure for multiple comparisons was employed to assess differences across genotypes (Vm rest Pre: ***$P < 0.00032$, Ba^{2+}: ns. $P =$

0.093, Post: ***$P < 0.00066$; rheobase Pre: *$P < 0.032$, Ba^{2+}: ns. $P = 0.723$, Post: ns. $P = 0.025$; Rin Pre: **$P < 0.0032$, Ba^{2+}: $P = 0.891$, Post **$P < 0.0066$).

In Fig. **S5B**, control $n = 4$ and Th^{Kir} $n = 4$. In Fig. **S5C**, Student's *t*-test.

In Fig. **S6A**, Student's t-test or Mann-Whitney *U*-test corrected with the FDR procedure for multiple comparisons at peri-threshold intensity (Emb: ns. $P = 0.141$, P0-1: **$P < 0.005$, P2-3: *$P < 0.0375$, P4-7: *$P < 0.0125$). Student's *t*-test or the Mann-Whitney *U*-test corrected with the FDR procedure for multiple comparisons at 500μA (Emb: ns. $P = 0.502$, P0-1: ns. $P = 0.631$, P2-3: *$P < 0.025$, P4-7: *$P< 0.0125$). In Fig. **S6C**, Hyperbolic curve fitting using a nonlinear least square regression analysis, fitted parameters from control and Th^{Kir} datasets were compared with a global fit using Extra Sum-of-squares F Test method.

In Fig. **S6D**, Student's *t*-test or the Mann-Whitney *U*-test corrected with the FDR procedure for multiple comparisons (+ side Emb: ns. $P = 0.192$, P0-1: ns. $P = 0.452$, P2-3: *$P < 0.0125$, P4-7: *$P < 0.025$; - side Emb: ns $P = 0.173$, P0-1: ns. $P = 0.180$, P2-3: *$P < 0.025$, P4-7: **$P < 0.0025$).

In Fig. **S7C**, stimulation 200 μA. Student's *t*-test corrected with the FDR procedure for multiple comparisons (Emb: *$P < 0.025$, P0-1 ns. $P = 0.104$, P2-3: ns. $P = 0.4$, P4-5 **$P < 0.0025$).

In Fig. **S8B**, Student's *t*-test. *$P < 0.05$. In Fig. **S8D**, Two-way ANOVA test. For cortical area activated P0-2: $F_{genotype} = 3.619$, ns. $P = 0.067$; $F_{stim} = 13.693$, *** $P < 0.001$; for $\Delta F/F_0$ of area activated P0-2: $F_{genotype} = 4.277$, * $P < 0.047$; $F_{stim} = 5.047$, * $P < 0.013$. For cortical area activated P4-5: $F_{genotype} = 37.468$, ns. *** $P < 0.001$; $F_{stim} = 2.628$, ns. $P = 0.089$; for $\Delta F/F_0$ of area activated P4-5: $F_{genotype} = 21.576$, *** $P < 0.001$; $F_{stim} = 1.568$, ns. $P = 0.225$; interactions across factors was not significant in any case. In Fig. **S8E**, Student's *t*-test corrected with the FDR procedure for multiple comparisons (P0-2 + side: **$P < 0.01$, P3-5 (+) side: **$P < 0.005$; P0-2 – side: ns. $P = 0.344$, P3-5 (–) side: **$P < 0.005$. In Fig. **S8F,** $n = 3$.

In Fig. **S9B,** Student's *t*-test. In Fig. **S9E,** Onset Latency: Two-way ANOVA test and Tuckey's multiple comparisons test; Initial Peak Current, Current Area -70mV and 50mV: Two-way ANOVA test and Sidak's multiple comparisons test for comparing means only between control and Th^{Kir}.

In Fig. **S10C**, Quantification of the horizontal width of the cortical response measured as the length where fluorescence drops 50% with respect to the initiation site. Repeated measures two-way ANOVA test and Bonferroni's multiple comparisons test. In Fig. **S10D**, Student's *t*-test.

In Fig. **S11A**, control and Th^{Kir} $n = 4$. In Fig. **S11B**, $n = 3$. In Fig. **S11C**, control and Th^{Kir} $n = 3$.

In Fig. **S12B**, Student's *t*-test corrected with the FDR procedure for multiple comparisons (Vm P0-1: $^{**}P < 0.0075$, P2-3: $^{***}P < 0.0003$, P6-8: $^{***}P < 0.0005$, P15-17: ns $P = 0.078$; rheobase P0-1: $^{*}P < 0.0375$, P2-3: $^{***}P < 0.00025$, P6-8: $^{*}P < 0.05$, P15-17: $^{*}P < 0.025$; Rin P0-1: $^{*}P < 0.0375$, P2-3: $^{***}P < 0.0003$, P6-8: $^{**}P < 0.005$, P15-17: ns. $P = 0.064$). In Fig. **S12E**, maximal responses (Student's *t*-test, $P = 0.494$) and latency (Student's *t*-test, $P = 0.4937$). In Fig. **S12F**, Mann-Whitney *U*-test.

In Fig. **S13A**, control, $n = 8$ and Th^{Kir}, $n = 6$. In Fig. **S13C**, control, $n = 3$ and Th^{Kir}, $n = 3$. In Fig. **S13D**, control, $n = 10$ and Th^{Kir}, $n = 10$.

In Fig. **S15A**, left: control and Th^{Kir}, $n = 5$. Right, control and Th^{Kir}, $n = 3$. In Fig. **S15B**, control and Th^{Kir}, $n = 3$. In Fig. **S15C**, $control_{C2\text{-}whisker}$ and $control_{no\text{-}whiskers}$ $n = 3$.

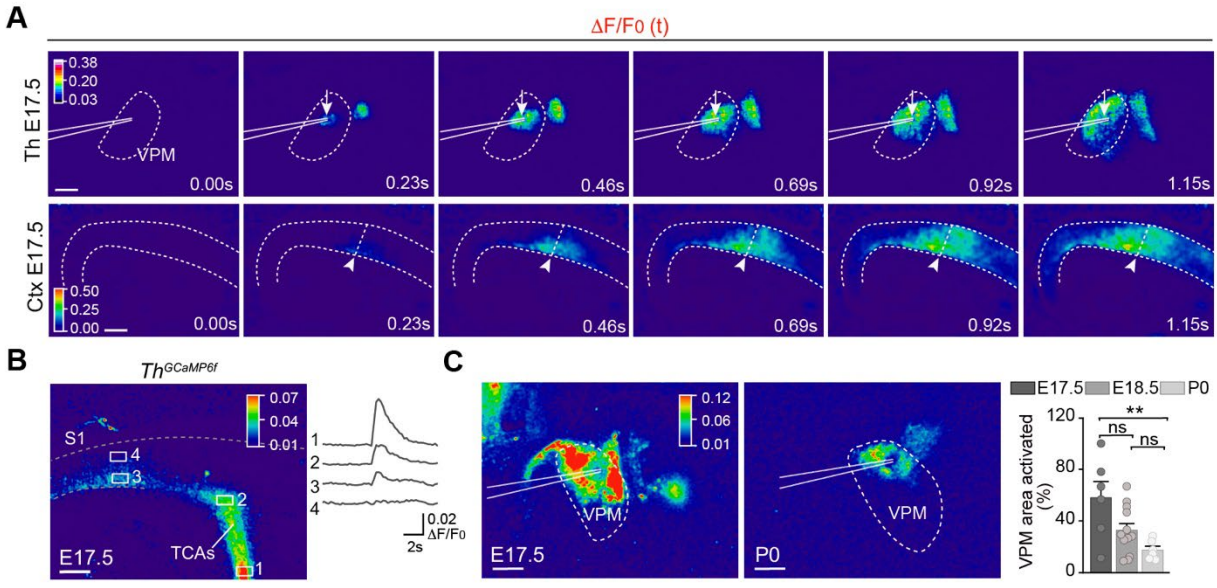

Fig.S1. Time course of thalamic and cortical activation after ventral postero-medial nucleus (VPM) stimulation. (**A**) Propagation of thalamic and cortical calcium responses evoked by a 125 µA pulse in the VPM of a E17.5 slice loaded with Cal520 (same example as in Figure 1A). The response origin is indicated with an arrow in the thalamus and an arrowhead in the cortex. (**B**) Maximal projection of the calcium response in thalamocortical axons after VPM stimulation (300 µA) in a $Th^{GCaMP6f}$ mouse at E17.5. (**C**) Thalamic calcium responses elicited after VPM stimulation in an E17.5 and P0 mice. Quantification of the data shown in left panels (E17.5 n = 6 slices from 5 mice; E18.5 n = 12 slices from 10 mice; P0 n = 6 slices from 5 mice. E17.5 vs. E18.5: ns. P = 0.061, E18.5 vs. P0: ns. P = 0.329, E17.5 vs. P0: $^{**}P < 0.01$). S1, primary somatosensory cortex. Scale bars, 200 µm. Data are means ± SEM.

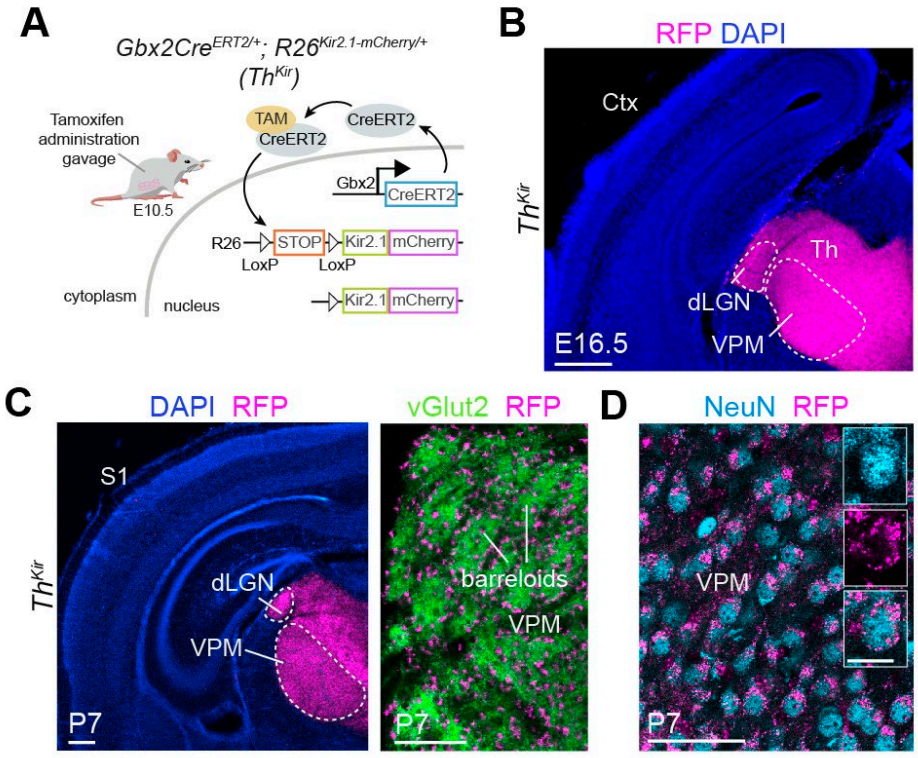

Fig.S2. Selective overexpression of Kir2.1 in the thalamus in the *Th^{Kir}* mouse. (**A**) Scheme of the genetic conditional overexpression of Kir2.1 in thalamic neurons upon tamoxifen (TAM). Kir2.1 is fused to the mCherry reporter protein. (**B**) Coronal section at E16.5 showing Kir2.1-mCherry expression after tamoxifen administration at E10.5. Recombination is restricted to the thalamus (Th) within the forebrain and absent in the cortex (Ctx). (**C**) Coronal sections showing Kir2.1 overexpression (RFP) in the *Th^{Kir}* mice and in barreloids immunostained with vGlut2 at P7. (**D**) RFP-positive neurons immunostained with NeuN in *Th^{Kir}* thalamus at P7. dLGN, dorsal-lateral geniculate nucleus; VPM, ventral postero-medial nucleus. S1, primary somatosensory cortex. Scale bars, 300 µm in **B** and **C** (left); 100 µm in **C** (right); 50 µm in **D** (insets: 12.5 µm).

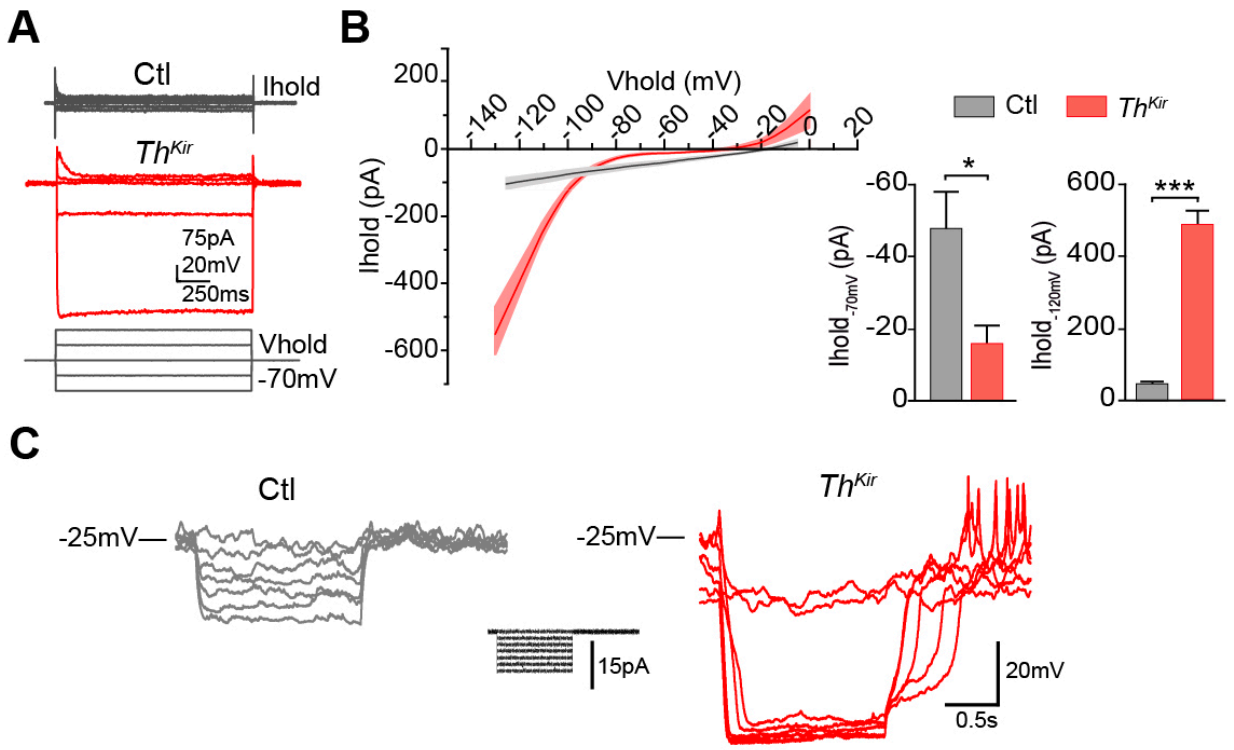

Fig.S3. ***Ex vivo*** **electrophysiological properties of** ***Th^{Kir}*** **ventral postero-medial (VPM) neurons at E16.5.** (**A**) Responses to a family of voltage steps from a holding potential of -70 mV in a control and a *Th^{Kir}* neuron. (**B**) Current-voltage relationship (I-V curve) in control and *Th^{Kir}* thalamic cells. Cells were held at -70 mV and pulses of 1500 ms in 10 mV steps increment were delivered (range -120 to -10 mV). Notice the strong inward rectification in the *Th^{Kir}* sample, as expected for cells expressing a high Kir2.1 conductance. Right: Quantification of the holding current required to keep Vm at -70 mV and -120 mV in control (n = 5) and *Th^{Kir}* cells (n = 7). *P < 0.05, ***P < 0.001. (**C**) Injection of low-amplitude (< 20 pA) current pulses induced Vm oscillations in embryonic *Th^{Kir}* neurons. Data are means ± SEM.

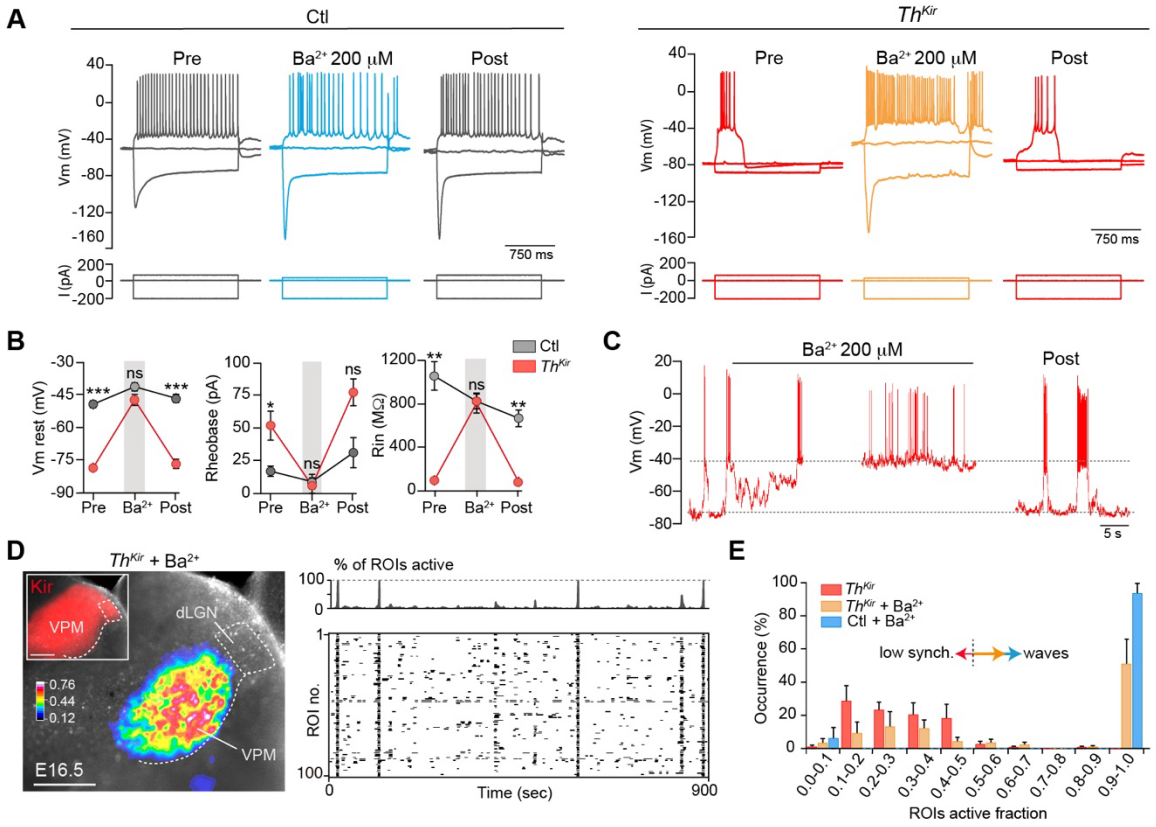

Fig. S4. Blocking Kir2.1 conductance with barium reverts the electrophysiological properties and calcium wave activity in the *Th*^{Kir} mice. (**A**) Representative examples of the membrane voltage (Vm) responses to a family of current steps in P3 control and *Th*^{Kir} neurons perfused with ACSF (pre) and ACSF plus barium (Ba^{2+}; 200 µM), and after washout (post). (**B**) Quantification of the effects of Ba^{2+} on the resting Vm, rheobase and input resistance (Rin). Control, $n = 5$ and *Th*^{Kir}, $n = 5$ neurons from P0-P8; ns. not significant; $*P < 0.05$, $**P < 0.01$, $***P < 0.001$. (**C**) Representative traces of the effect of Ba^{2+} (200 µM) on the Vm in *Th*^{Kir} neurons. (**D**) Representative example of the effect of Ba^{2+} (50 µM) on the spontaneous calcium activity in the *Th*^{Kir} mice. Calcium waves reappear when Kir channels are blocked. (**E**) Frequency distribution

of the active ROI fraction in the VPM in control + Ba^{2+}, Th^{Kir} and Th^{Kir} + Ba^{2+}. Data were obtained from $n = 4$, $n = 7$ and $n = 5$ experiments, respectively. Scale bar, 200 μm. Data are means ± SEM.

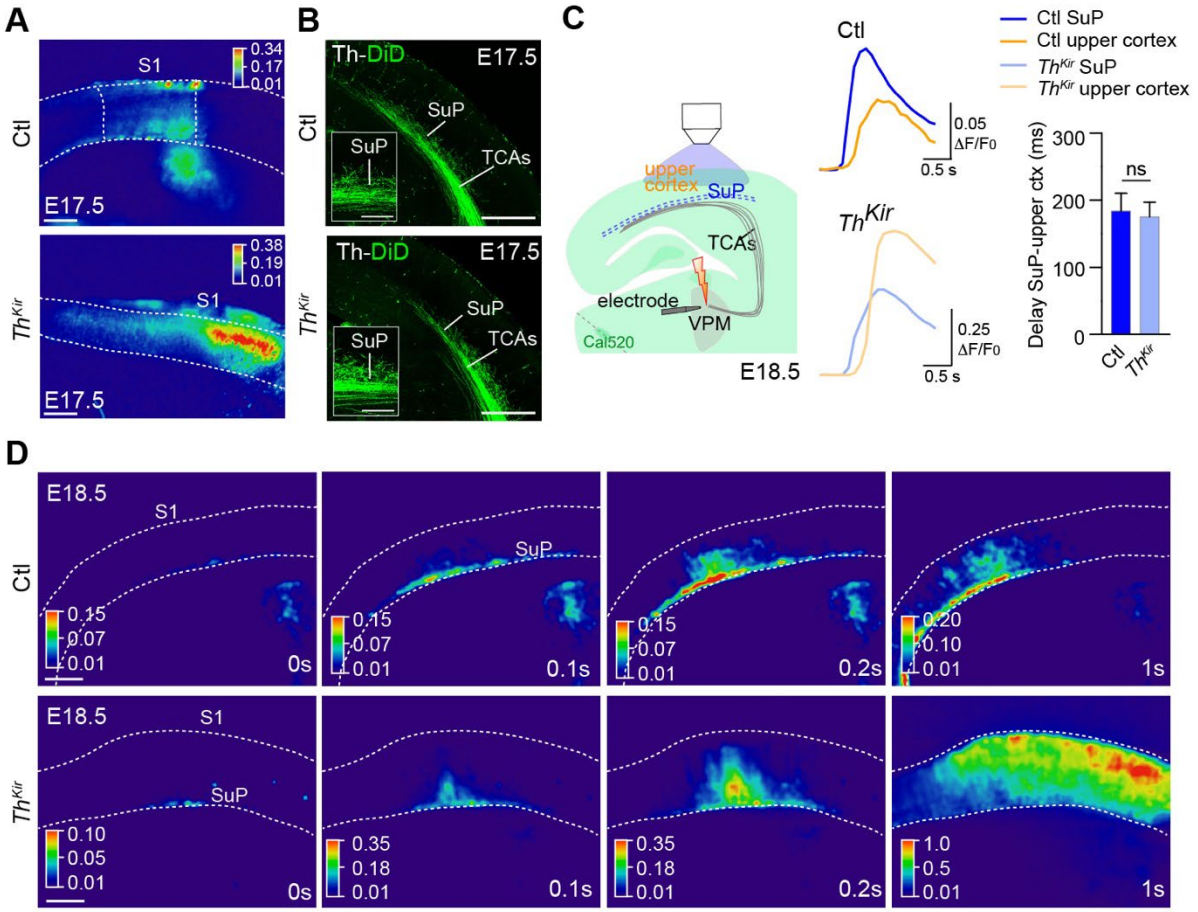

Fig.S5. Widespread embryonic cortical activity and subplate/upper cortex activation delay. (**A**) Maximal projection of the cortical activation elicited by peri-threshold ventral postero-medial nucleus (VPM) stimulation in control and *Th*^{Kir} slices at E17.5 (**B**) Coronal sections showing thalamocortical axons (TCAs) labeled with DiD at E17.5 in control and *Th*^{Kir} mice. (**C**) Experimental design and representative calcium traces. Cortical activation occurs first at the subplate (SuP) level followed by the upper cortex in both control and *Th*^{Kir} mice. Quantification of the delay in both conditions (n = 4 control, n = 7 *Th*^{Kir}, ns. not significant P = 0.806). (**D**) Temporal sequence of cortical activation in the SuP followed by the upper cortex in both control and *Th*^{Kir} mice. S1, primary somatosensory cortex. Scale bars, 200 µm. Data are means ± SEM.

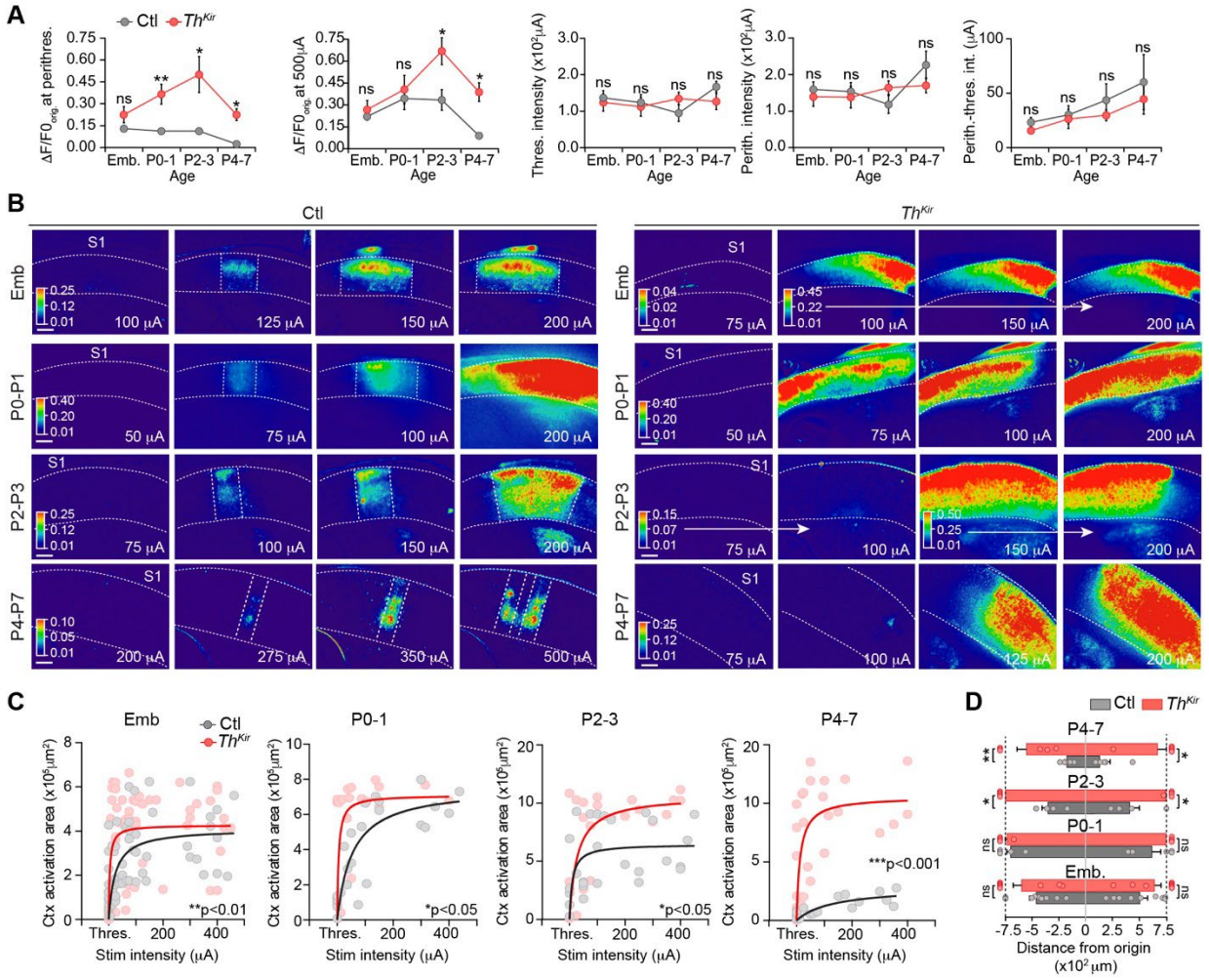

Fig.S6. The development of functional cortical pre-barrel columns is hindered in the *Th*^{Kir} mice. (**A**) Quantification of the developmental profile of cortical calcium signals measured at response origin ($\Delta F/F_0$ at origin) after peri-threshold and maximal ventral postero-medial nucleus (VPM) stimulation in slices (E17.5 $n = 9$ control and $n = 9$ *Th*^{Kir}; P0-1 $n = 5$ control and $n = 4$ *Th*^{Kir}; P2-3 $n = 5$ control and $n = 5$ *Th*^{Kir}; P4-7 $n = 6$ control and $n = 7$ *Th*^{Kir}). Quantification of the threshold, peri-threshold and peri-thershold minus threshold intensities (see "Quantification" section for p values). (**B**) Maximal projection of the cortical response evoked by VPM stimulation at increasing intensities within the same slice at distinct developmental stages in control and *Th*^{Kir}.

White arrows indicate images with the same pseudocolor scale. (**C**) Quantification of the cortical activation area evoked by increasing stimulus intensities at different developmental stages (E17.5 n = 14 control and n = 13 Th^{Kir}; P0-1 n = 6 control and n = 5 Th^{Kir}; P2-3 n = 5 control and n = 5 Th^{Kir}; P4-7 n = 6 control and n = 7 Th^{Kir}). (**D**) Quantification of the spreading of the cortical calcium activation in response to maximal stimulation in control and Th^{Kir} slices at different developmental stages. Bars represent the extent of activation, measured as the distance from response initiation to the position where fluorescence decays to half. Red points lying beyond the vertical dashed lines correspond to calcium waves that spread out of the visual field (± 750 µm from the origin). E17.5 n = 9 control and n = 9 Th^{Kir}; P0-1 n = 5 control and n = 4 Th^{Kir}; P2-3 n = 5 control and n = 5 Th^{Kir}; P4-7 n = 6 control and n = 7 Th^{Kir}. S1, primary somatosensory cortex. Scale bars, 200 µm. Data are means ± SEM.

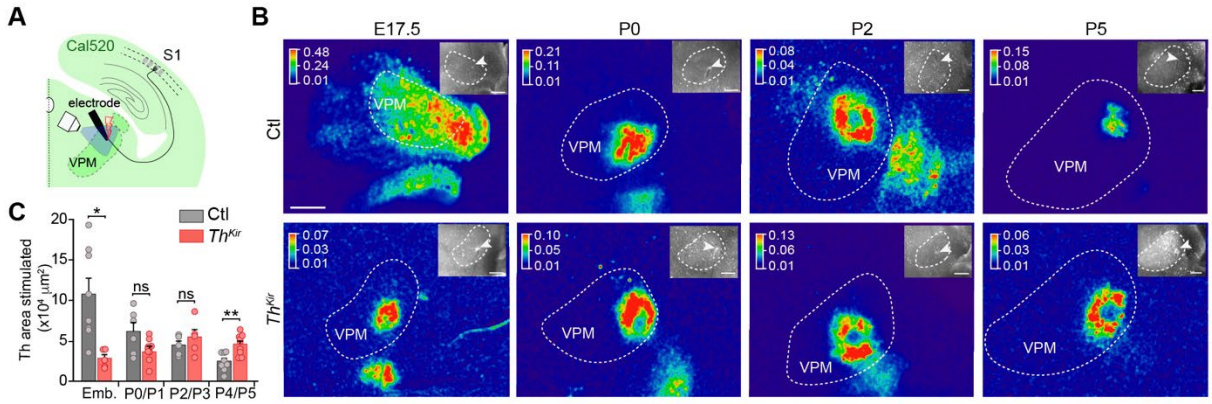

Fig.S7. Extensive cortical activation in *Th*^{Kir} mice is not due to an increment in the area of the ventral postero-medial nucleus (VPM) response recruited by the stimulus. (**A**) Experimental design. (**B**) Maximum projection of the calcium responses upon VPM stimulation (200 µA) in control and *Th*^{Kir} slices at distinct developmental time points. Arrowheads in insets indicate the position of the electrode. (**C**) Quantification of the thalamic stimulated area at different developmental stages (E17.5: $n = 8$ control, $n = 5$ *Th*^{Kir}; P0-1: $n = 6$ control, $n = 9$ *Th*^{Kir}; P2-3: $n = 5$ control, $n = 5$ *Th*^{Kir}; P4-5: $n = 8$ control, $n = 9$ *Th*^{Kir}; $*P < 0.05$, P0-1 ns. $P = 0.104$, P2-3: ns. $P = 0.4$, P4-5 $**P < 0.01$). Scale bars, 200 µm. Data are means ± SEM.

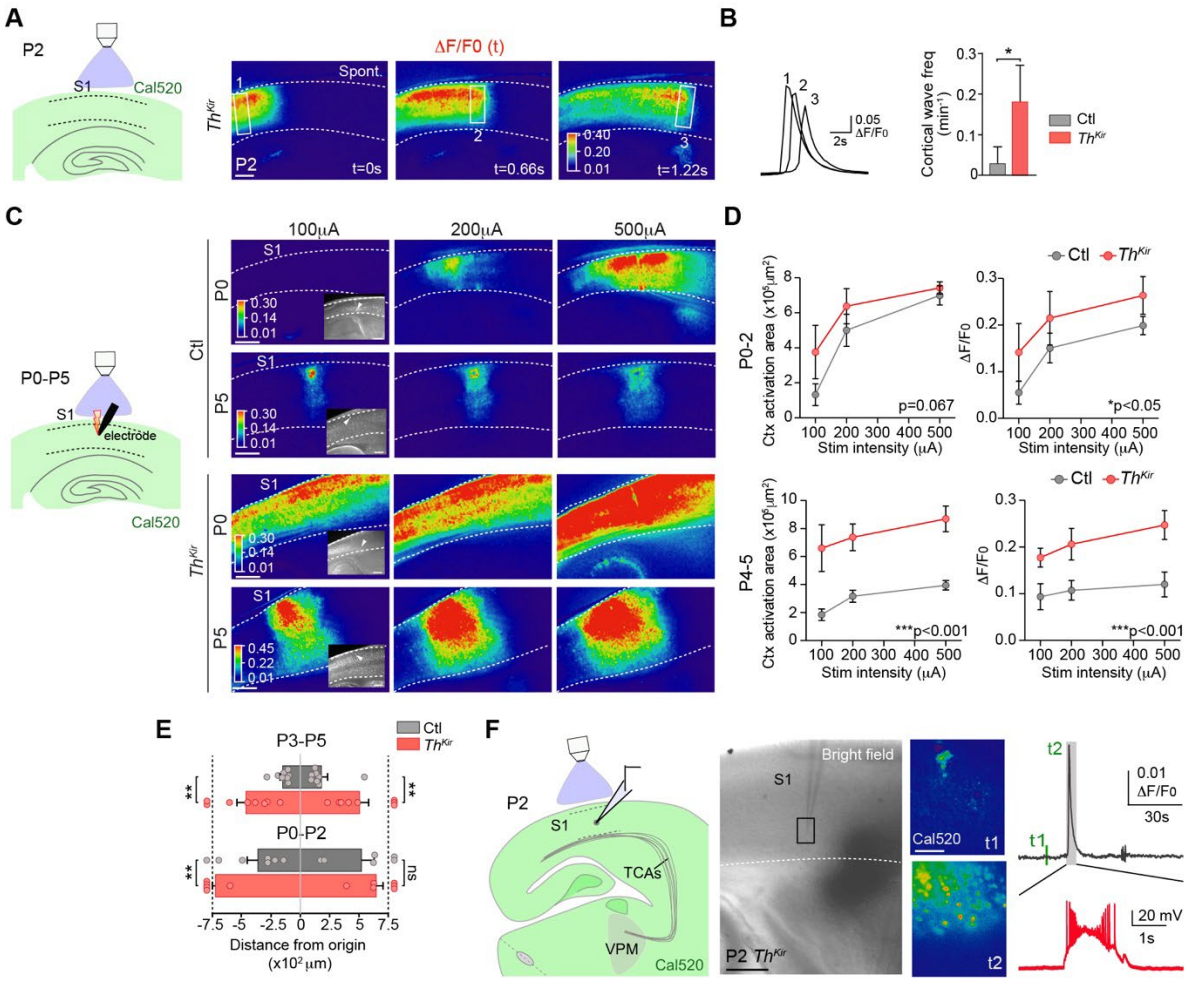

Fig.S8. Prenatal switch of spontaneous thalamic activity modifies intrinsic cortical excitability. (**A**) Experimental design. Maximum projection of the spread in time of a spontaneous cortical wave in a P2 Th^{Kir} slice. (**B**) Time course of the calcium transients in the ROIs and quantification of spontaneous wave frequency in control (n = 6) and Th^{Kir} (n = 6). (**C**) Experimental design. Maximum projection of the cortical calcium responses upon cortical stimulation at different intensities at P0 and P5 in control and Th^{Kir} mice. (**D**) Quantification of the area and intensity of the cortical response evoked by increasing stimulus amplitudes (control: n = 6 P0-2 and n = 6 P4-5 slices; Th^{Kir}: n = 6 P0-2 and n = 6 P4-5 slices). (**E**) Quantification of the horizontal spreading of the response at 200µA. Bars represent the extent of activation measured as

the distance from response initiation site to the position where fluorescence decays to half. Red points lying beyond the vertical dashed lines correspond to calcium waves that spread out of the visual field (± 750 μm from the origin). P0-2 $n = 6$ control and Th^{Kir} slices, P3-5 $n = 8$ control and Th^{Kir} slices. (**F**) Experimental design. Simultaneous acquisition of calcium and current-clamp responses during spontaneous activity in cortical neurons. Spontaneous cortical waves in the Th^{Kir} mice are associated with a transient burst of action potentials in cortical neurons ($n = 3$). S1, primary somatosensory cortex. Scale bars, 200 μm. Data are means ± SEM.

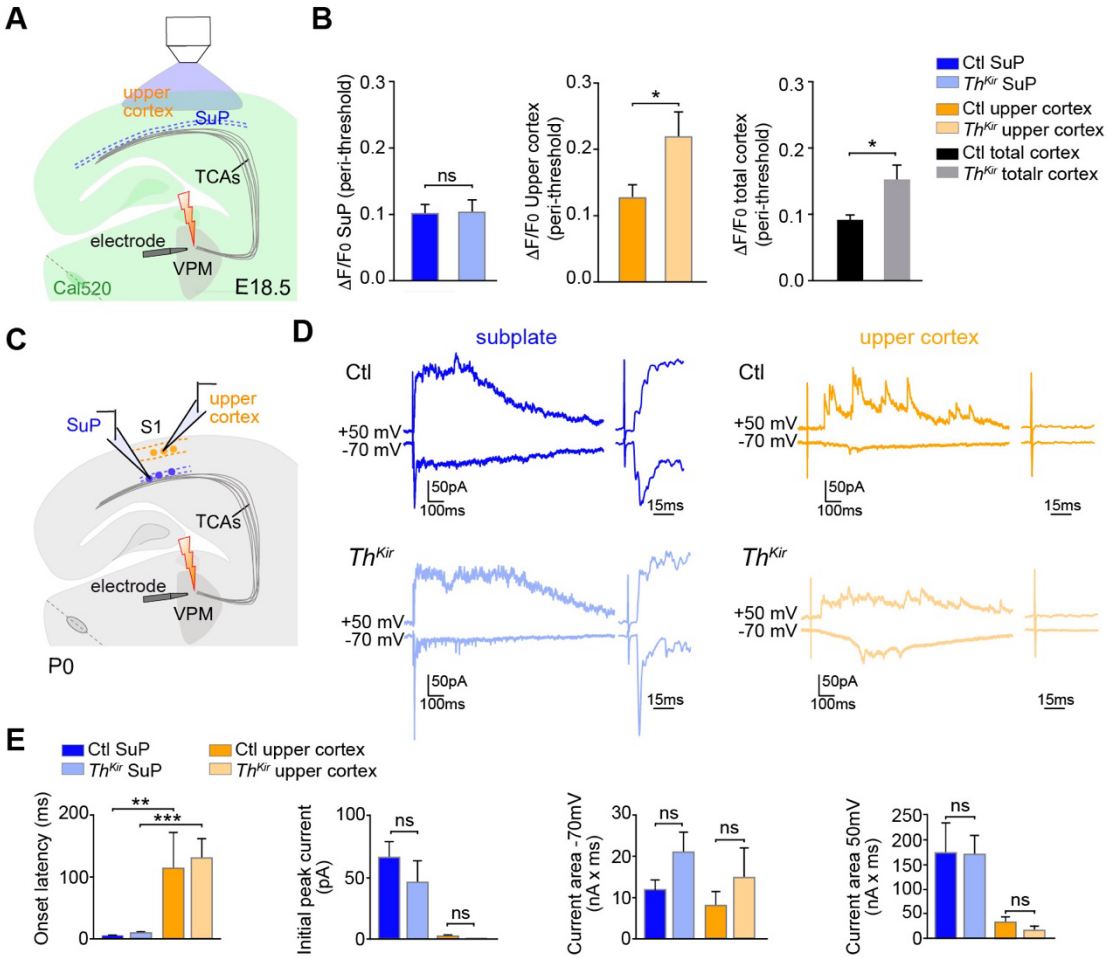

Fig.S9. Calcium dynamics and current properties in subplate (SuP) and upper cortex. (A) Experimental paradigm. (**B**) Quantification of the $\Delta F/F_0$ at peri-threshold stimulation in SuP, upper cortex and total cortical wall in control and *Th*^{Kir} mice at E18.5 (control, n = 14; *Th*^{Kir} n = 13; $\Delta F/F_0$ Subplate ns. P = 0.934; $*P < 0.05$). (**C**) Experimental design. (**D**) Traces showing the excitatory postsynaptic currents (EPSCs) triggered in SuP and upper cortical neurons held at -70 mV and 50 mV after ventral postero-medial nucleus (VPM) stimulation. (**E**) Quantification of EPSC properties recorded from SuP and upper cortex neurons in control and *Th*^{Kir} mice at P0 (n = 5-14 control, n = 5-11 *Th*^{Kir}; Onset latency: $**P < 0.01$, $***P < 0.001$; Initial peak current: SuP ns. P = 0.511, Upper Cortex ns. P = 0.999; Current area -70 mV: SuP ns. P = 0.155, Upper cortex

ns. P = 0.587; Current area 50 mV: SuP ns. P = 0.999, Upper cortex ns. P = 0.975). S1, primary somatosensory cortex. Data are means ± SEM.

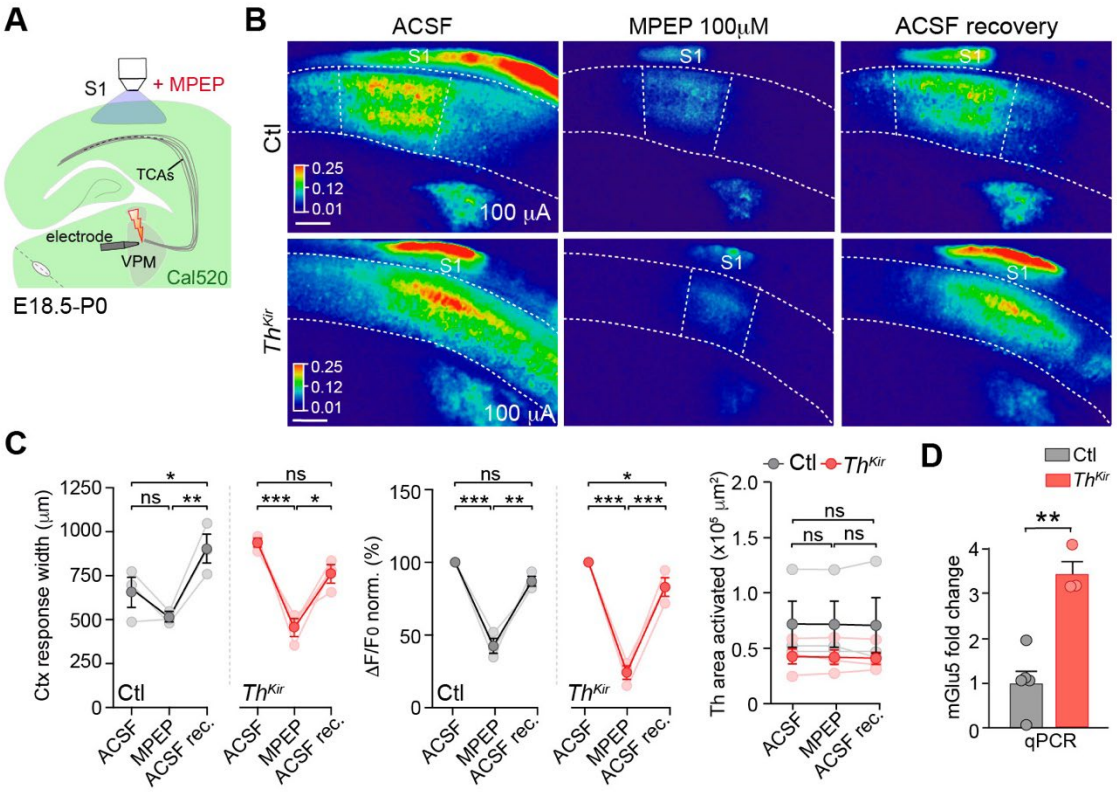

Fig.S10. Effect of mGlu5 antagonist in the thalamocortical-induced cortical response. (**A**) Experimental design. (**B**) Maximum projection of the cortical calcium responses upon ventral postero-medial nucleus (VPM) stimulation before, during and after application of the mGlu5 receptor antagonist MPEP (100 µM) at P0. **(C)** Quantification of the evoked calcium responses shown in B. Control (n = 3) and *Th*^{Kir} (n = 3) slices. For cortical response width: Control: ACSF vs. MPEP ns. (not significant) P = 0.226; *Th*^{Kir}: ACSF vs. ACSF recovery ns. P = 0.119; *P < 0.05; **P < 0.01; ***P < 0.001. For $\Delta F/F_0$: Control: ACSF vs. ACSF recovery ns. P = 0.134; *P < 0.05; **P < 0.01; ***P < 0.001. For Th area activated: Control: ACSF vs MPEP ns. P > 0.999; MPEP vs Recovery ns. P > 0.999; ACSF vs Recovery ns. P > 0.999; *Th*^{Kir}: ACSF vs MPEP ns. P = 0.998; MPEP vs Recovery ns. P = 0.997; ACSF vs Recovery ns. P = 0.991). Mean values are represented in darker circles. (**D**) Quantitative PCR for mGlu5 levels in the control (n = 5) and

Th^{Kir} (n = 3) mice at P0, **P < 0.01. Scale bars, 200 μm. S1, primary somatosensory cortex. Data are means ± SEM.

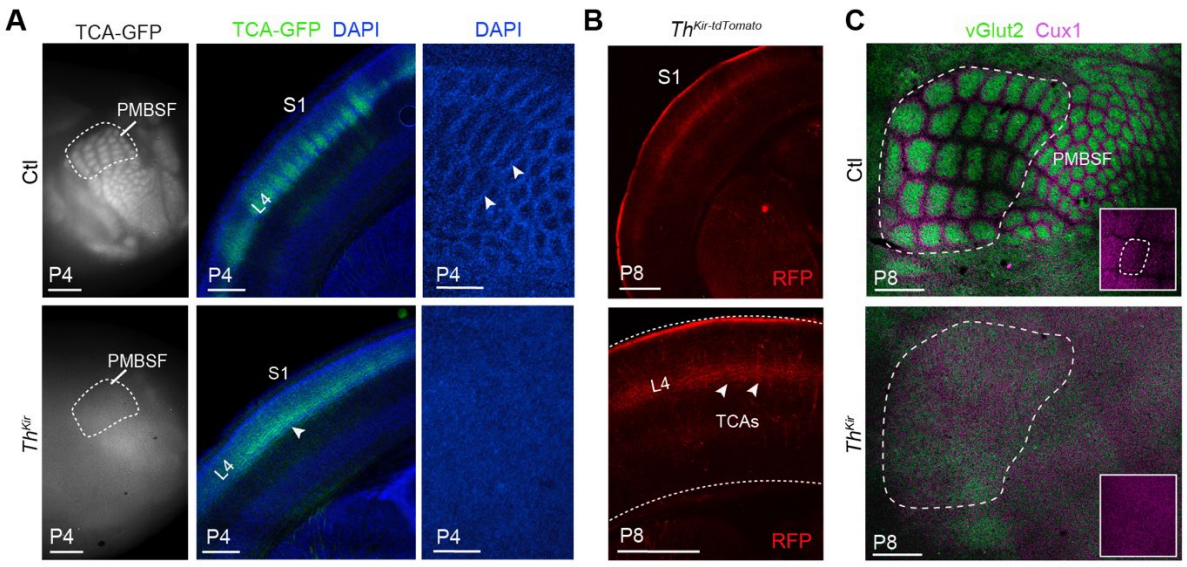

Fig.S11. Barrel map formation is compromised after disruption of thalamic waves. (A) *In toto* (left), coronal (middle) and tangential (right) view of the PMBSF map formation. In the TCA-GFP genetic background, TCAs are labeled in green at P4 in control and Th^{Kir} mice. DAPI (blue) shows the disposition of layer 4 (L4) neurons in the PMBSF. (**B**) Coronal section showing thalamocortical axon (TCAs) terminals expressing *Kir* (tdTomato) in the L4 of Th^{Kir} mice at P8. (**C**) Tangential view of the PMBSF sensory map representation at P8. vGlut2 immunostaining of TC terminals and of Cux1 immunostaining of cortical cells. Notice the lack of PMBSF map in Th^{Kir} mice. S1, primary somatosensory cortex. Scale bars, 1 mm in **A** (left panels) and 300 µm in **A** (middle/right panels), **B** and **C**.

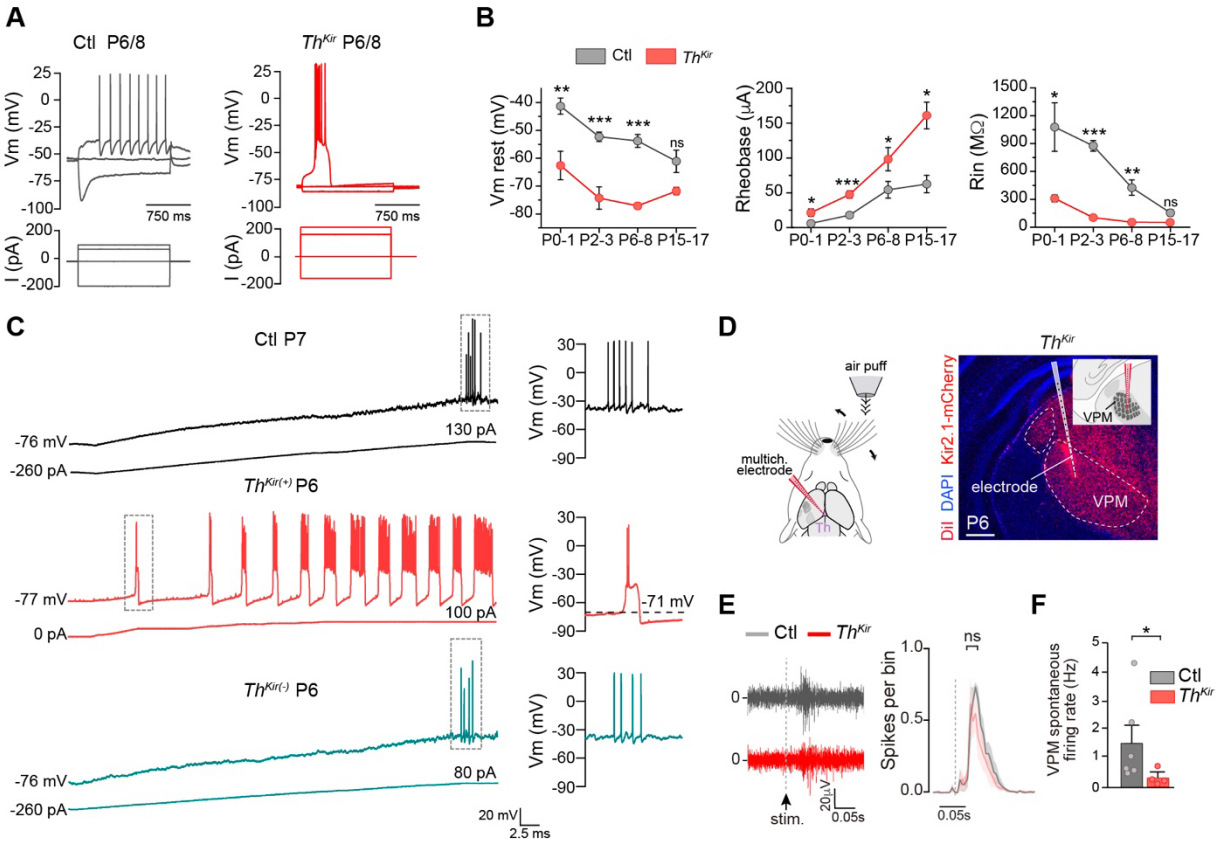

Fig.S12. *Ex vivo* and *in vivo* electrophysiological properties of ventral postero-medial nucleus (VPM) *Th*^{Kir} neurons during early postnatal development. (**A**) Representative examples of the voltage responses to a family of current steps in control and *Th*^{Kir} VPM cells at P6-P8. (**B**) Quantification of membrane potential (Vm), rheobase and membrane input resistance (Rin). $n = 4$ to 22 cells for each condition; $*P < 0.05$, $**P < 0.01$, $***P < 0.001$. (**C**) Voltage changes associated to a current ramp in control, *Th*^{Kir}-positive and *Th*^{Kir}-negative neurons. Note that Vm oscillates when reaches -71 mV in the *Th*^{Kir}. (**D**) Experimental design and coronal section counterstained with DAPI showing the electrode labeled with DiI. (**E**) Representative examples of VPM multi-unit activity (MUA) evoked by whisker stimulation in control ($n = 4$) and *Th*^{Kir} ($n = 4$). Dashed line represents the onset of the stimulus (time = 0). Right: Quantification of number of spikes per

5 ms bin. (**F**) Quantification of the spontaneous firing rate in the VPM of control ($n = 6$) and Th^{Kir} ($n = 4$) mice. *$P < 0.05$. Scale bar, 300 μm. Data are means ± SEM.

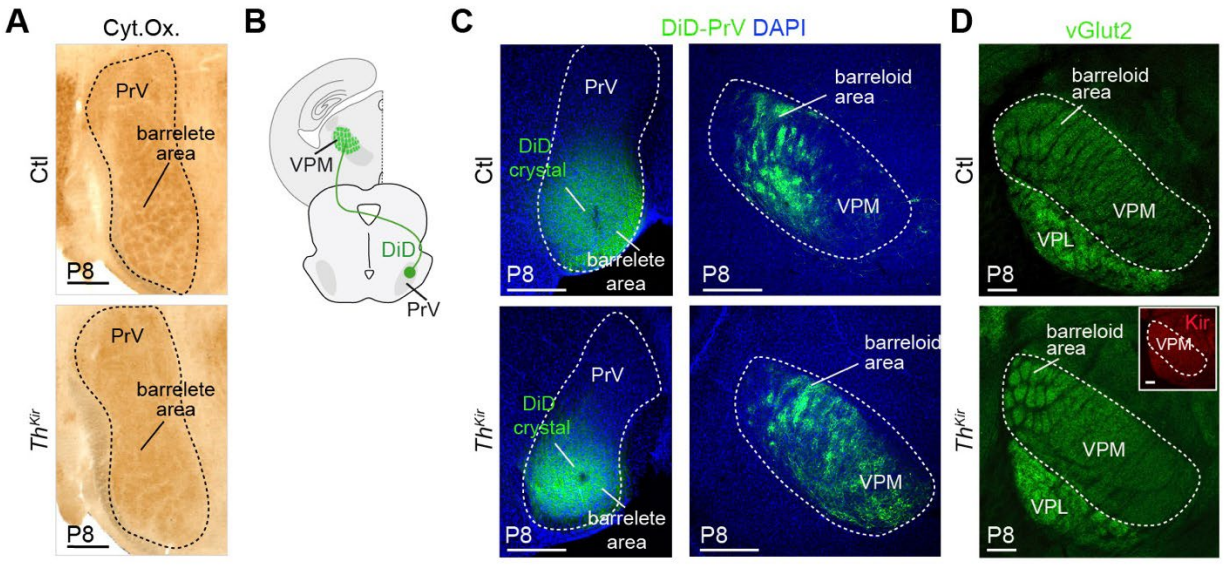

Fig.S13. Subcortical structures are not affected in *Th*^{Kir} mice. (**A**) Representative images of cytocrome Oxidase (Cyt. Ox.) staining showing the barrelettes in the principal sensory trigeminal nucleus (PrV) of the hindbrain in control and *Th*^{Kir} mice at P8. (**B**) Experimental design. (**C**) Representative images of DiD crystal localization in the PrV (left panels) in control and *Th*^{Kir}. Right: Coronal sections showing PrV axons targeting the ventral postero-medial nucleus (VPM) in both control and *Th*^{Kir} mice at P8. (**D**) Coronal view of the VPM labeled with vGlut2 in both control and *Th*^{Kir} mice at P8. Notice the presence of barreloids in *Th*^{Kir}. Scale bars, 300 µm.

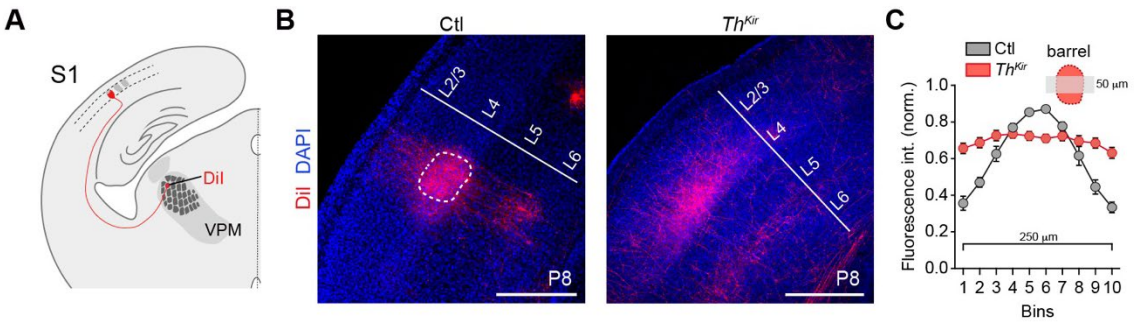

Fig.S14. Thalamocortical axons do not cluster in *Th*^{Kir} mice. (**A**) Experimental design. A small DiI crystal was placed in the barreloid area of the ventral postero-medial nucleus (VPM). (**B**) Coronal sections showing thalamocortical axons clusters labelled with DiI forming barrels in control mice. TCAs are horizontally oriented at the layer 4 (L4) in *Th*^{Kir} mice. (**C**) Quantification of the fluorescence intensity in L4 (250 x 50 µm ROI) normalized by the maximum intensity of each sample in control (n = 13) and *Th*^{Kir} (n = 21) mice. Each bin represents 25 µm (total: 250 µm). S1, primary somatosensory cortex. Scale bars, 300 µm. Data are means ± SEM.

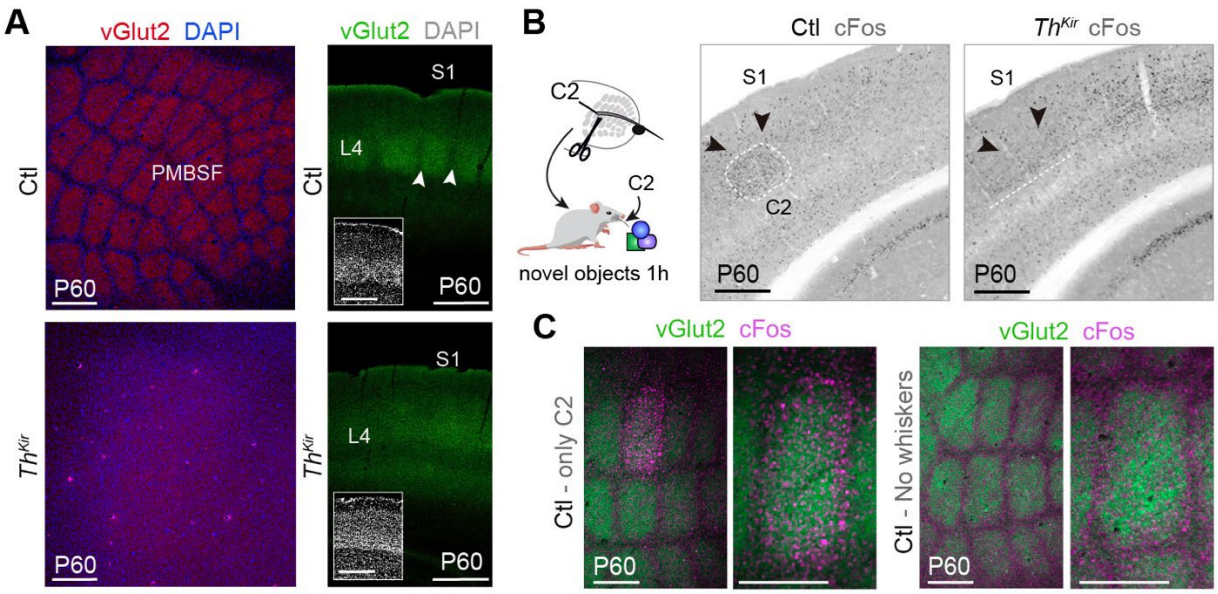

Fig.S15. Functional disruption of the map representation in adult *Th*^{Kir} mice. (**A**) Flattened tangential sections immunolabeled for vGlut2 in the adult PMBSF control and *Th*^{Kir} mice. Right: Coronal sections showing vGlut2 immunolabeling in the primary somatosensory cortex (S1) of control and *Th*^{Kir} mice at P60. Insets show DAPI staining. (**B**) Experimental design. Animals were kept 1 hour in the open field arena with distinct novel objects. Prior to the novelty exposure test, all whiskers were trimmed except C2. Right: Coronal sections showing cFos immunolabeling in control and *Th*^{Kir} mice. Note C2 activation in the control S1. (**C**) Tangential sections of the PMBSF somatosensory map stained by vGlut2 and cFos immunostaining in control mice. L4, layer 4. Scale bars, 300 μm.

Movie S1. Example of the cortical response elicited by VPM stimulation (125 μA, 0.2 ms) at E17.5. Calcium concentration is represented in pseudocolor. 1x speed, 110 ms interframe interval.

Movie S2. Representative example of *in vivo* cortical calcium responses elicited after peripheral stimulation in an $Emx1^{Cre/+};R26^{GCaMP6f/+}$ embryo at E18.5. 1x speed, 300 ms interframe interval.

Movie S3. Representative example of a control spontaneous thalamic activity at E16.5. Calcium concentration is represented in pseudocolor. Real interframe interval: 300 ms.

Movie S4. Representative example of thalamic activity in a Th^{Kir} mouse at E16.5. Calcium concentration is represented in pseudocolor. 30x speed, 300 ms interframe interval.

Movie S5. Representative example of the thalamic activity after Ba^{2+} (50 μM) in a Th^{Kir} mouse at E16.5. Calcium concentration is represented in pseudocolor. 1x speed, 300 ms interframe interval.

Movie S6. Cortical calcium response elicited in a control E18.5 mouse after VPM stimulation. Calcium concentration is represented in pseudocolor. 1x speed, 300 ms interframe interval.

Movie S7. Cortical calcium response elicited in a Th^{Kir} mouse at E17.5 after peri-threshold VPM stimulation. Calcium concentration is represented in pseudocolor. 1x speed, 230 ms interframe interval.

Movie S8. Cortical calcium response elicited in a Th^{Kir} mouse at E18.5 after peri-threshold VPM stimulation. Calcium concentration is represented in pseudocolor. 1x speed, 230 ms interframe interval.

Movie S9. Cortical calcium response elicited in a control P2 mouse after peri-threshold VPM stimulation. Calcium concentration is represented in pseudocolor. 1x speed, 230 ms interframe interval.

Movie S10. Cortical calcium response elicited in a Th^{Kir} mouse at P2 after peri-threshold VPM stimulation. Calcium concentration is represented in pseudocolor. 1x speed, 230 ms interframe interval.

Movie S11. Representative example of *in vivo* cortical calcium responses elicited after peripheral stimulation in a Thy1-control P4 mouse. 1x speed, 300 ms interframe interval.

Movie S12. Representative example of *in vivo* cortical calcium responses elicited after peripheral stimulation in a *Thy1-*Th^{Kir} P4 mouse. 1x speed, 300 ms interframe interval.

References

1. V. B. Mountcastle, *J Neurophysiol* **20**, 408-434 (1957).
2. P. Rakic, *Science* **241**, 170-176 (1988).
3. D. H. Hubel, T. N. Wiesel, *J Physiol* **160**, 106-154 (1962).
4. P. Rakic, A. E. Ayoub, J. J. Breunig, M. H. Dominguez, *Trends Neurosci* **32**, 291-301 (2009).
5. A. Tiriac, B. E. Smith, M. B. Feller, *Neuron*, (2018).
6. T. K. Hensch, *Annu Rev Neurosci* **27**, 549-579 (2004).
7. P. Gaspar, N. Renier, *Curr Opin Neurobiol* **53**, 43-49 (2018).
8. H. P. Killackey, G. Belford, R. Ryugo, D. K. Ryugo, *Brain Res* **104**, 309-315 (1976).
9. T. A. Woolsey, J. R. Wann, *J Comp Neurol* **170**, 53-66 (1976).
10. V. Moreno-Juan *et al.*, *Nat Commun* **8**, 14172 (2017).
11. T. A. Woolsey, H. Van der Loos, *Brain Res* **17**, 205-242 (1970).
12. A. Agmon, L. T. Yang, E. G. Jones, D. K. O'Dowd, *J Neurosci* **15**, 549-561 (1995).
13. J. W. Yang *et al.*, *Cereb Cortex* **23**, 1299-1316 (2013).
14. H. Mizuno *et al.*, *Cell Rep* **22**, 123-135 (2018).
15. O. Mitrukhina, D. Suchkov, R. Khazipov, M. Minlebaev, *Cereb Cortex* **25**, 3458-3467 (2015).
16. N. Alagem, M. Dvir, E. Reuveny, *J Physiol* **534**, 381-393 (2001).
17. J. Wagner, H. J. Luhmann, *Neuropharmacology* **51**, 848-857 (2006).
18. D. P. Calderon, N. Leverkova, A. Peinado, *J Neurosci* **25**, 1737-1749 (2005).
19. H. Mizuno *et al.*, *Neuron* **82**, 365-379 (2014).
20. R. S. Erzurumlu, P. Gaspar, *Eur J Neurosci* **35**, 1540-1553 (2012).
21. H. Li *et al.*, *Neuron* **79**, 970-986 (2013).
22. N. Narboux-Neme *et al.*, *Journal of Neuroscience* **32**, 6183-6196 (2012).
23. H. Van der Loos, T. A. Woolsey, *Science* **179**, 395-398 (1973).
24. W. L. Weller, J. I. Johnson, *Brain Res* **83**, 504-508 (1975).
25. L. Lokmane, S. Garel, *Semin Cell Dev Biol* **35**, 147-155 (2014).
26. M. C. Crair, R. C. Malenka, *Nature* **375**, 325-328 (1995).
27. J. A. Gorski *et al.*, *J Neurosci* **22**, 6309-6314 (2002).
28. L. Chen, Q. Guo, J. Li, *Development* **136**, 1317-1326 (2009).
29. S. J. Franco *et al.*, *Science* **337**, 746-749 (2012).
30. E. Dupont, I. L. Hanganu, W. Kilb, S. Hirsch, H. J. Luhmann, *Nature* **439**, 79-83 (2006).
31. D. Curran-Everett, *Am J Physiol Regul Integr Comp Physiol* **279**, R1-8 (2000).